


RESEARCH ARTICLE

Open Access



Coupled investigations of ionosphere variations over European and Japanese regions: observations, comparative analysis, and validation of models and facilities

Sergii V. Panasenko^{1*} , Dmytro V. Kotov¹, Yuichi Otsuka², Mamoru Yamamoto³, Hiroyuki Hashiguchi³, Philip G. Richards⁴, Vladimir Truhlik⁵, Oleksandr V. Bogomaz¹, Maryna O. Shulha¹, Taras G. Zhivolup¹ and Igor F. Domnin¹

Abstract

This paper presents the results of a coordinated measurement campaign with ground based and satellite observations over European and Japanese regions during September 5–6, 2017. Two incoherent scatter radars, two satellite missions, International Reference Ionosphere (IRI-2016) empirical model, and Field Line Interhemispheric Plasma (FLIP) physical model were employed to examine the regular behavior of the F2-layer peak height and density and the topside ionosphere electron density, electron, and ion temperatures as well as traveling ionospheric disturbances (TIDs). The daily ionospheric variations over Kharkiv and Shigaraki exhibited similar behavior qualitatively and quantitatively. The results show that none of the empirical IRI-2016 models of F2-layer peak height, topside electron density, and temperature can be preferred for predicting the key qualitative features of variations in ionospheric plasma parameters over Kharkiv and Shigaraki. The likely reason is rapid day to day changes in solar activity and series of moderate enhancements of magnetic activity occurring in the observation period and preceding days. Compared with IRI-2016 model, the FLIP physical model was shown to provide the best agreement with the observations when constrained to follow the observed diurnal variations of F2-layer peak height both over Europe and Japan. This paper presents the first direct comparison of the mid-latitude electron density measured by the Swarm satellite with incoherent scatter radar data and it confirms the high quality of the space-borne data. For the first time, evidence of the possible need to increase the neutral hydrogen density in NRLMSISE-00 model by at least a factor of 2 was obtained for the Asian longitudinal sector. The TIDs, which have predominant periods of about 50 min over Europe and 80 min over Japan, were detected, likely caused by passage of the solar terminator. Such a difference in the periods could indicate regional features and is the topic for further research.

Keywords: Ionospheric observations, European and Japanese sectors, Background, storm-time, and wave-like variations, Model and facility validation

*Correspondence: sergii.v.panasenko@gmail.com

¹Institute of Ionosphere, 16 Kyrychova, Kharkiv 61001, Ukraine
Full list of author information is available at the end of the article

1 Introduction

Knowledge about the characteristics of geospace environment all over the world is necessary for understanding and predicting space weather phenomena during different solar and magnetic activity conditions. Strong space weather events such as severe and extreme magnetic storms are known to result in significant variations in ionosphere and thermosphere (IT) parameters and often have negative effects on human infrastructure, especially, on space-based assets (see, e.g., Hapgood (2011); Tsurutani et al. (2012)). Moreover, there is evidence that even weak changes in parameters of the solar wind and interplanetary magnetic field can profoundly affect the ionosphere and plasmasphere. In particular, Buresova et al. (2014) revealed that minor and moderate storms occurring during very low solar activity conditions can cause variations in the F2 peak electron density (N_mF2) and height (h_mF2) that can rival those observed during strong magnetic activity. Kotov et al. (2018); Kotov et al. (2019) reported a significant decrease (factor of 2) in plasmaspheric density that was induced by a very weak magnetic disturbance and strong modulation of the ionosphere-plasmasphere H^+ ion fluxes that causes strong variations in the ion composition of the topside ionosphere. The magnitude of the observed effects depends highly on the amount of energy transferred to the magnetosphere and ionosphere and also on the previous and current state of the IT system, its regional features, and time of storm onset. Trigger mechanisms of energy release can also play a decisive role due to the highly nonlinear IT response to the external influence (Chernogor 2011).

Tides and gravity waves propagating from low altitudes also contribute to ionospheric variability. For example, solar tides propagating into the low latitude dynamo region induce electric fields that produce the so-called wave 4 crest structure of enhanced neutral and plasma density (Sagawa et al. 2005; England et al. 2006).

In situ and remote sensing provide reliable information about the IT characteristics which can be measured but the data are sparse in both the temporal and/or spatial domain. On the other hand, models can reproduce the temporal variations of IT parameters over a definite location, but they may not reflect reality. This is caused by the lack of the data on which empirical models are based or incomplete knowledge about input or embedded parameter values used for physical models. For example, there are discrepancies between International Reference Ionosphere (IRI) model predictions and experimental results occurring for definite regions (see, e.g., Liu et al. (2019); Patel et al. (2019)). One way to reduce these differences is to use data assimilation models that account for diurnal and regional variability (e.g., Schunk et al. (2014)). Recent investigations confirmed that

the Field Line Interhemispheric Plasma (FLIP) model can reproduce the ionospheric and plasmaspheric variability over the East-European region for all seasons (Kotov et al. 2015, 2016, 2018, 2019). It is important that in those studies the FLIP model was constrained to follow the observed h_mF2 variations.

Numerous experimental and theoretical studies have established that there are strong latitudinal differences of IT processes, thereby clearly separating the aeronomy, dynamics, and electrodynamics of polar, mid-latitude and equatorial regions (e.g., Heelis (2004); Kim et al. (2020)). Such variability arises from latitudinal changes of solar radiative heating, atmosphere composition, and circulation, as well as the geomagnetic field configuration. Even longitudinal dependencies of the IT processes occurring during the same local time are not fully understood since they are greatly influenced by the displacement of geographic and geomagnetic poles. The East-Siberian magnetic anomaly is known to be responsible for strong longitudinal variations of N_mF2 in the Northern Hemisphere polar ionosphere (Pirog et al. 2001), whereas the electron density in the Southern Hemisphere has regional features such as the Weddell Sea anomaly (Luan and Dou 2013; Richards et al. 2017). Zhang et al. (2011); Zhang et al. (2012) detected an east-west difference in the electron density over the continental United States using GPS receiver and Millstone Hill incoherent scatter radar (ISR) data.

Panasenko et al. (2018) studied background and wave-like variations in ionospheric characteristics over the East-American and European sectors (distant by ~ 108 degrees of longitude) from joint measurements using two mid-latitude Kharkiv and Millstone-Hill ISRs. They found considerable differences in the magnitude of both diurnal and quasi-periodic variations in electron density and ion and electron temperatures over ISR locations which cannot be simply interpreted in terms of dependence on magnetic and/or geographic coordinates.

This work is an extension of our investigation of regional differences in the mid-latitude ionosphere. Here, we present a comparative analysis for European and Japanese regions (separated by ~ 100 degrees of longitude). The results from ground based and satellite observations as well as ionospheric and plasmaspheric model simulations are analyzed with the aim of revealing of the regional differences and validating the empirical and physical models.

The advantage of this study is the use of data from a special joint observation campaign conducted with ISRs located at Kharkiv (Europe) and Shigaraki (Japan). Both radars were the only mid-latitude European and Asian ISRs that operated simultaneously during the period of 5–6 September 2017. As magnetic activity moderately increased on September 6, it enabled a study of

the longitudinal effects of a weak magnetic storm and tested the capability of models to reproduce the storm effects.

2 Geospace state, facilities, models, and methods

Coordinated observations of the background, wave-like, and storm-induced ionospheric variations were conducted using the Kharkiv ISR (KhISR) and the Shigaraki MU radar (MUR) during 5–6 September 2017. These stations are at mid geographic latitudes but different magnetic latitudes. KhISR is located in the north-east of Ukraine at (49.6° N, 36.3° E). The Shigaraki MUR is located at Shigaraki MU observatory, Shigaraki, Japan at (34.9° N, 136.1° E). The Kharkiv magnetic latitude is 45.5°, with a dip angle of 66.6°. The Shigaraki magnetic latitude is 26.2° with a 49.1° dip angle.

2.1 Solar and magnetic conditions

The measurements were made 5–6 September 2017 prior to the onset of the severe magnetic storm of 7–8 September 2017. Though the observations were near the minimum phase of the solar cycle (average $F_{10.7}$ index ~ 83), September 1–6 were characterized by enhanced $F_{10.7}$ solar flux and sunspot number values with the $F_{10.7}$ index maximizing at 183 at 20 UT on September 4 (Fig. 1). Figure 1 also shows that magnetic disturbances occurred with maximum K and K_p values equal to 5 late on September 4. A series of separate bursts of the AE index occurred during September 5–6 reaching up to ~ 800 nT on September 6 morning.

2.2 Radar measurements

The Kharkiv radar characteristics, operating modes, and software suites for data analysis were described by

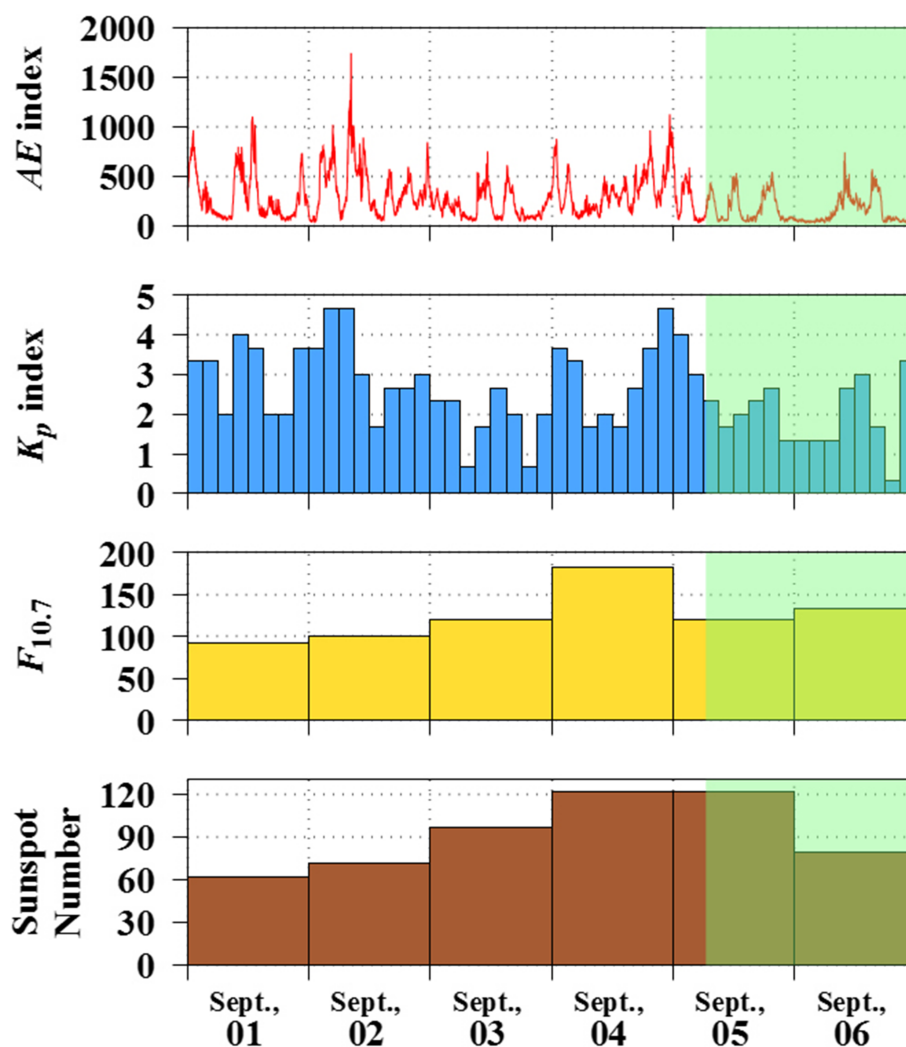


Fig. 1 Variations of sunspot number, solar flux $F_{10.7}$, planetary index K_p , and AE index during 1–6 September 2017. Green shaded area denotes the ionospheric measuring campaign period. Time is UT

Domnin et al. (2014) and Bogomaz et al. (2017) and are on the website (<http://iion.org.ua>).

For this study, KhISR operated in a composite two-frequency radio pulse mode. The first simple pulse has a length of about $650 \mu\text{s}$ (the carrier frequency $f_0=158 \text{ MHz}$), providing an altitude resolution of $\sim 100 \text{ km}$, while the second simple one has the pulse length of about $135 \mu\text{s}$ (the frequency $f_1=(158+0.1) \text{ MHz}$) and yields the 20-km altitude resolution. As a result of receiving and processing of the first signal element scattered by the ionosphere, the electron density, the electron and ion temperatures, the vertical component of the plasma velocity, and the ion composition are measured for the altitudes near the peak of the ionospheric F2 layer and in the upper ionosphere. The return signal from the second pulse element allows the determination of the altitude profile of the IS signal power (P_s) at the altitudes $h=100\text{--}550 \text{ km}$ for correction of the altitude electron density profile and estimation of vertical propagation characteristics of traveling ionospheric disturbances (TIDs) such as vertical phase velocity and wavelength.

The Shigaraki MUR operated at a frequency of 46.5 MHz (Fukao et al. 1985, 1985; Hassenpflug et al. 2008). It is a fully active phased array system which employs up to four independent beams and realizes sequential sensing toward the magnetic north, east, south and west. Standard IS modes are usually used for ionospheric parameter retrieval of the electron density and ion drift velocity as well as ion and electron temperatures (see, e.g., Table 1 from Balan et al. (1998)).

During the joint measuring campaign, the MU radar was operated in a modified mode with only one beam directed toward the magnetic south to provide consistency between the ISR and MU results. Two different pulse patterns (7-element code) were transmitted. The pattern “1000000,” where “1” means a presence and “0” means an absence of a single subpulse being of $96 \mu\text{s}$ width, was employed for signal power. Another pattern “1100101” enabled the estimation of autocorrelation functions for retrieving ion and electron temperatures. The patterns alternated approximately every 5 min (52 sets of 512 scans with 11 ms interpulse period). Data were acquired starting at $1333 \mu\text{s}$ after the pattern transmission onset. This provided a lower boundary at a distance of 200 km corresponding to 188 km altitude for an antenna beam zenith angle is 20° . Only data obtained during the “1000000” pattern transmission were analyzed further in this paper.

The electron densities measured by both radars were calibrated using the data of ionosondes located nearby.

2.3 Satellite data

2.3.1 DMSP satellite data

DMSP is a mission of the United States Air Force that currently consist of four satellites (F15–F18) flying in circular Sun-synchronous, polar orbits at altitudes between 820 and 860 km (Hairston et al. 2018).

The DMSP spacecraft measure several plasma parameters in the topside ionosphere with the special sensor-ion, electron, scintillation (SSIES) package consisting of the following thermal plasma instruments: Langmuir probe, retarding potential analyzer, scintillation monitor, and ion drift meter (Heelis and Hanson 1998; Rich 1994; Brace 1998).

This study used the electron density, and electron and ion temperatures from all F15–F18 DMSP satellites. Only the data points with good quality flags were used. The DMSP F15 electron density data quality was previously validated for the KhISR region (Kotov et al. 2018).

2.3.2 Swarm Langmuir probe data

Swarm is a mission of the European Space Agency primarily intended to study the Earth’s magnetic field. The mission has a constellation of three satellites named A, B, and C which were deployed into circular near-polar low Earth orbits at the end of 2013.

Swarm A and C orbit side-by-side at the same altitude at $\sim 460 \text{ km}$ (inclination 87.4°) and Swarm B flies at an altitude of about 530 km (inclination 88°). All the satellites are equipped with identical instruments. This study used Level 1b 2 Hz time resolution data from the Langmuir probes (Knudsen et al. 2017). The data are downloadable from <https://swarm-diss.eo.esa.int/>.

This study uses the high-quality electron density data from all three Swarm satellites. These data were recently validated by comparison with ISR measurements (excluding KhISR and MUR) by Lomidze et al. (2018). Other satellite instruments and models (IRI) indicated that Swarm typically underestimates the electron density by 10–15%.

The Swarm electron temperatures were not used for this study as recent validation studies have reported that the Swarm Langmuir probe electron temperatures can be greatly overestimated. Lomidze et al. (2018) proposed a calibration of measured electron temperature using comparisons with ISR measurements. However, some problems with the data quality remain including unpredictable jumps along the satellite orbits.

2.4 Ionospheric models

2.4.1 FLIP model

The field line interhemispheric plasma (FLIP) model is a one-dimensional model that calculates the plasma den-

sities and temperatures along magnetic flux tubes from below 100 km in the Northern Hemisphere through the plasmasphere to below 100 km in the Southern Hemisphere (Richards 2001; Richards et al. 2010). A detailed description of the FLIP model can be found in the paper of Kotov et al. (2015).

Due to a lack of direct measurements, neutral winds are one of the greatest uncertainties for modeling ionosphere electron densities. The FLIP model overcomes this problem by adjusting the neutral winds to accurately reproduce the observed h_mF2 when available (Richards 1991). The FLIP model can also use empirical model h_mF2 or neutral winds such as from the HWM-14 wind model (Drob et al. 2015). All the model runs were conducted with the actual values of solar and magnetic activity indices.

2.4.2 Models of electron and ion temperatures

The International Reference Ionosphere model (IRI) includes a global description of the electron temperature (T_e). Beginning from IRI-2012, the TBT-2012 model is the default option for the topside (Truhlik et al. 2012; Bilitza et al. 2014). The model employs a spherical harmonics representation of the electron temperature at several fixed altitudes where most satellite data is available (350, 550, 850, 1400, and 2000 km) providing different sets of coefficients for different seasons. As the modeling coordinates, the magnetic local time and a special latitudinal magnetic coordinate invdip were used (Truhlik et al. 2001). A Booker function (Booker 1977) was employed to describe the altitude variation of T_e . The TBT-2012 model provides a more detailed description of the diurnal variation, including the morning overshoot, than previous models and includes an option to describe the variation of the electron temperature with solar activity (TBT-2012+SA).

The ion temperature (T_i) model in IRI was described by Bilitza (1990). The model is based on the latitudinal profiles from AEROS-A satellite measured at 430 km altitude.

2.4.3 F2 peak models

The IRI model provides two choices for the description of the F2 critical frequency f_oF2 : (1) the model recommended by the International Radio Consultative Committee (CCIR, 1967) and (2) the one proposed by the International Union of Radio Science (URSI) (Rush 1989). In this paper, we compare the observed peak electron density with values calculated with URSI version set as default at IRI-2016 site. The model predictions depend on the solar activity. Additionally, the F peak storm model (Fuller-Rowell et al. 1998, 2000) was turned on to reflect average storms behavior in N_mF2 based on the A_p history over the preceding 33 h.

The F2 peak height is represented in IRI-2016 by three options: (1) from the correlation with the propagation

parameter $M(3000)F2$ (Bilitza et al. 1979), (2) the F2 peak height data from the worldwide ionosonde network (Altadill et al. 2013) (ATMB-2013), and (3) from the COSMIC radio occultation measurements (Shubin 2015) (SHU-2015). The SHU-2015 option seems to be the best choice following from several recent comparison studies. In this study, we compared the observations with the SHU-2015 and ATMB-2013 models. Both the models are governed by solar activity indices and they are insensitive to the changes in magnetic activity.

2.4.4 Topside electron density models

The IRI model includes three options for the electron density from the F2 peak up to 2000 km altitude with an extension to high altitudes into the plasmasphere for possible comparisons with GPS TEC. The electron density profiles from the topside models are normalized to N_mF2 .

The first option (IRI-2001) is based on the Bent model (Bent et al. 1972). The Bent model construction employed a limited amount of topside data that was available at the time (40,000 Alouetter-1 profiles). Numerous studies with other data have found it significantly overestimates the electron density in the upper topside (above ~ 500 km above h_mF2) increasing with altitude and reaching a factor of ~ 3 at 1000 km above the peak. For this reason, the IRI-01corr was introduced by Bilitza (2004) as a correction to the original version as a second option. The third option, which has been included since IRI-2007 as the default option for the topside ionosphere, adopts the topside electron density formulation of the NeQuik model (Nava et al. 2008).

2.5 Data analysis

The KhISR and MUR data were subjected to several processing stages using similar methods and procedures to ensure consistency between results. The data were first filtered to remove narrow bursts or spikes caused by the signal reflections from man-made objects like satellites, space debris, and from temporal variations in KhISR and MUR signal. We primarily estimated a signal-to-noise ratio (ratio of powers of incoherent scatter signal and noise, SNR) and an electron density vs time and altitude. Figure 2 shows that the SNR for the MUR data does not reach 0.1 and is up to two orders of magnitude less than that for KhISR. This causes the need to average the measured MUR signal parameters over substantially longer time intervals than those usually used for KhISR. To provide uniformity of the data of both radars in terms of temporal resolutions that is important for the correct comparison of the observational results, we averaged the ISR data over 3-h intervals. We ran FLIP model with h_mF2 variations obtained by KhISR with usual 20 min resolution and after 3-h averaging to check the possible additional errors in the FLIP plasma parameters

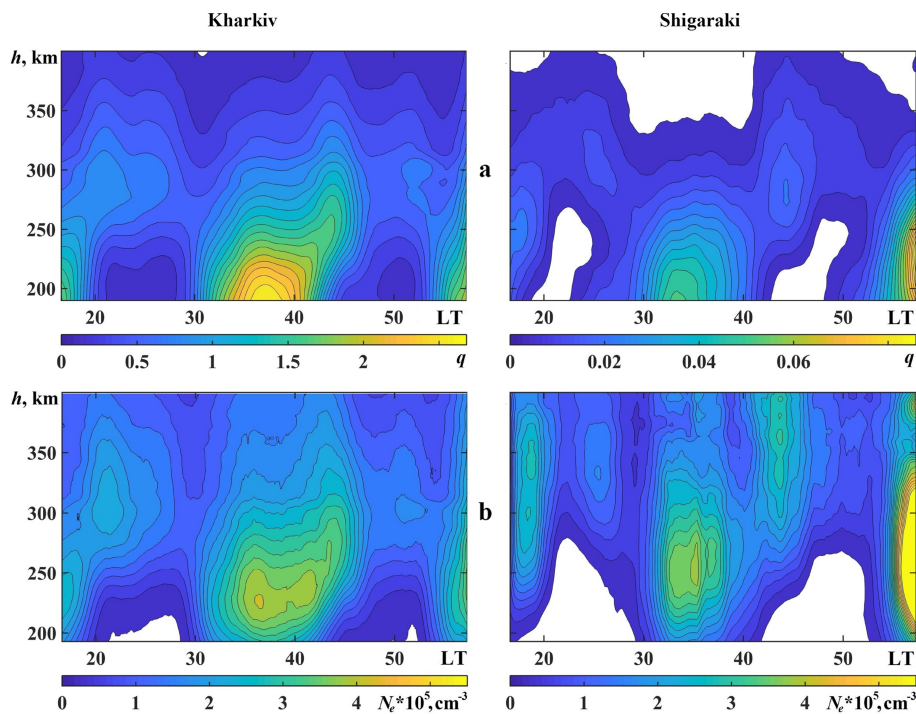


Fig. 2 Signal-to-noise ratio (top) and electron density (bottom) behavior over Kharkiv and Shigaraki during joint measuring campaign on 5–6 September 2017. LT is solar apparent time

related to the averaging. The errors are typically 3–5% and never exceed 10%. It is likely that the same applies for MUR data.

We applied a program package called UPRISE (Bogomaz et al. 2017) to retrieve ion and electron temperatures from the KhISR data but the MUR SNR was too low to retrieve temperatures (see above). As with the electron density averaging, the temporal variations of the ion and electron temperatures were smoothed over 3-h intervals as were all plasma parameters computed by the ionospheric models.

The KhISR electron and ion temperatures were retrieved from the auto-correlation functions. In the case of MUR, the temperatures were provided by the FLIP model, which are consistent with those obtained by DMSP satellites as seen below.

The electron density was evaluated using the measured IS signal power as well as electron and ion temperatures by algorithm described in the detail by Evans (1969).

Apart from background variations in ionospheric parameters, we detected quasiperiodic fluctuations in the electron density using spectral analysis. For this, the relative variations of the KhISR and MUR power were obtained as differences between the initial data and those after 3-h averaging, which were normalized to these average values. The adaptive Fourier

transform, which uses a sliding window with a variable width to be constantly equal to three harmonic period lengths (Chernogor 2008), was done to estimate the periods of predominant oscillations. The data analysis stages are described in detail by Panasenko et al. (2018), but 2-h data averaging was used in that paper.

3 Results

3.1 Comparison of observations in the European and Japanese longitudinal sectors

Figure 2 shows the diurnal and altitude variations of electron density obtained over Kharkiv and Shigaraki. Despite the extremely low SNR for the MUR data, the 3-h averaged N_e variations over Shigaraki demonstrate physically realistic behavior. The peak electron density exhibited similar values $(\sim 1\text{--}5) \times 10^5 \text{ cm}^{-3}$ over both sites. The main difference was observed in the local time morning on September 6 (near 56 LT) where the Shigaraki N_e was up to a factor of 2 greater than N_e over Kharkiv.

Figure 3 shows diurnal variations of the key ionospheric parameters – $h_m F2$ and $N_m F2$. The magnitude of the diurnal change of $h_m F2$ is largest for Shigaraki. During the daytime, the $h_m F2$ at Kharkiv is up to ~ 20 km higher than at Shigaraki, whereas during the nighttime, the reverse is true. Another prominent difference is the much stronger

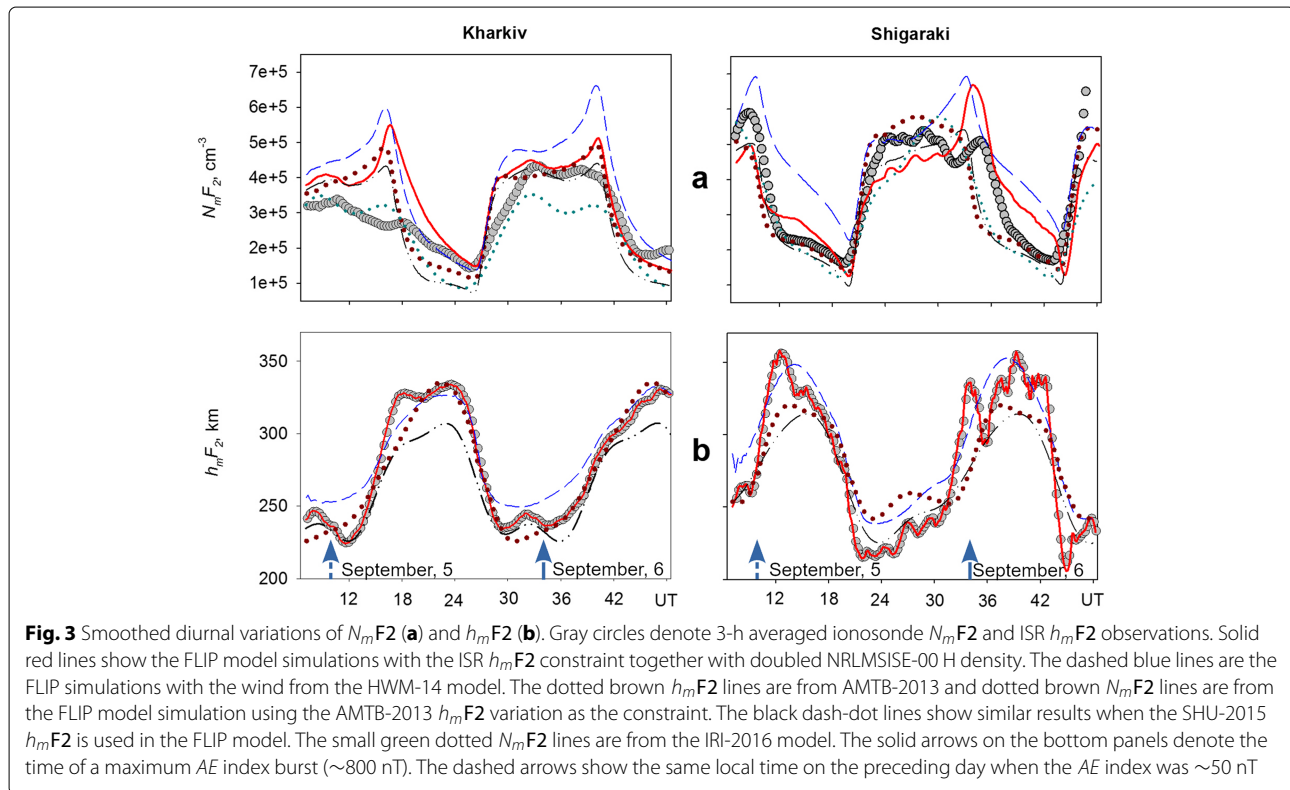


Fig. 3 Smoothed diurnal variations of N_mF2 (a) and h_mF2 (b). Gray circles denote 3-h averaged ionosonde N_mF2 and ISR h_mF2 observations. Solid red lines show the FLIP model simulations with the ISR h_mF2 constraint together with doubled NRLMSISE-00 H density. The dashed blue lines are the FLIP simulations with the wind from the HWM-14 model. The dotted brown h_mF2 lines are from AMTB-2013 and dotted brown N_mF2 lines are from the FLIP model simulation using the AMTB-2013 h_mF2 variation as the constraint. The black dash-dot lines show similar results when the SHU-2015 h_mF2 is used in the FLIP model. The small green dotted N_mF2 lines are from the IRI-2016 model. The solid arrows on the bottom panels denote the time of a maximum AE index burst (~ 800 nT). The dashed arrows show the same local time on the preceding day when the AE index was ~ 50 nT

variability of h_mF2 on a time scale of several hours for Shigaraki. The nighttime values of N_mF2 are close for both sectors ($\sim 2 \times 10^5 \text{ cm}^{-3}$) while the daytime N_mF2 is $\sim 30\%$ higher for Shigaraki. As in the case of h_mF2 , the N_mF2 variability on a time scale of several hours is stronger for Shigaraki. At Kharkiv, the measured N_mF2 is up to 50% lower for 12–18 UT than for 36–42 UT.

In the topside ionosphere, continuous diurnal variations of electron density were measured with KhISR but not with MUR because of the low SNR. Fortunately, four DMSP satellites provided daytime and nighttime data over both the European and Japanese regions at 850 km altitude (Fig. 4). At that altitude, the electron density is close to the FLIP model values over Kharkiv and Shigaraki for the daytime ($\sim 2.5 \times 10^4 \text{ cm}^{-3}$) and nighttime ($\sim 1.5 \times 10^4 \text{ cm}^{-3}$). The daytime DMSP electron temperature over Kharkiv is up to $\sim 25\%$ higher than over Shigaraki. The daytime DMSP and FLIP ion temperatures are also close for both sites (~ 2400 – 2700 K). Several data points for the electron density observed at lower orbits (508 km and 445 km) by three Swarm satellites show excellent agreement with the KhISR electron density data (Fig. 4d, e).

3.2 Comparison of observations with empirical model predictions

Figures 3 and 4 include a comparison of the observed variations of ionospheric plasma parameters with the

predictions of the sub-models of International Reference Ionosphere model.

The diurnal variation of the F2-layer peak density predicted by the N_mF2 model in IRI (Fig. 3a) is consistent with the Shigaraki ionosonde data except after 33 UT. Over Kharkiv, the IRI model underestimates N_mF2 by ~ 70 – 100% during nighttime and by $\sim 30\%$ during daytime on September 6 but not on September 5.

Both IRI h_mF2 models provide reasonable qualitative agreement with the observations in the European and Japanese regions (Fig. 3b). However, neither one can be preferred in terms of quantitative agreement with the data. The SHU-2015 model variation is much closer to the observations during daytime but it underestimates h_mF2 by ~ 20 – 30 km during nighttime. In contrast, the AMTB-2013 model predictions are better for the nighttime (especially for Europe) while the daytime h_mF2 values are ~ 25 km overestimated for Japan.

The two IRI electron temperature models underestimate the DMSP T_e during the daytime (Fig. 4a). In the European sector, the underestimation is ~ 600 – 1100 K for TBT-2012 without the solar activity (SA) option and ~ 1000 – 1500 K with the option. In the Japanese sector, the TBT-2012 model underestimates T_e by ~ 300 – 350 K while the SA option underestimates T_e by ~ 650 – 1100 K. The absence of nighttime DMSP T_e data precludes the evaluation of the model accuracy at Kharkiv.

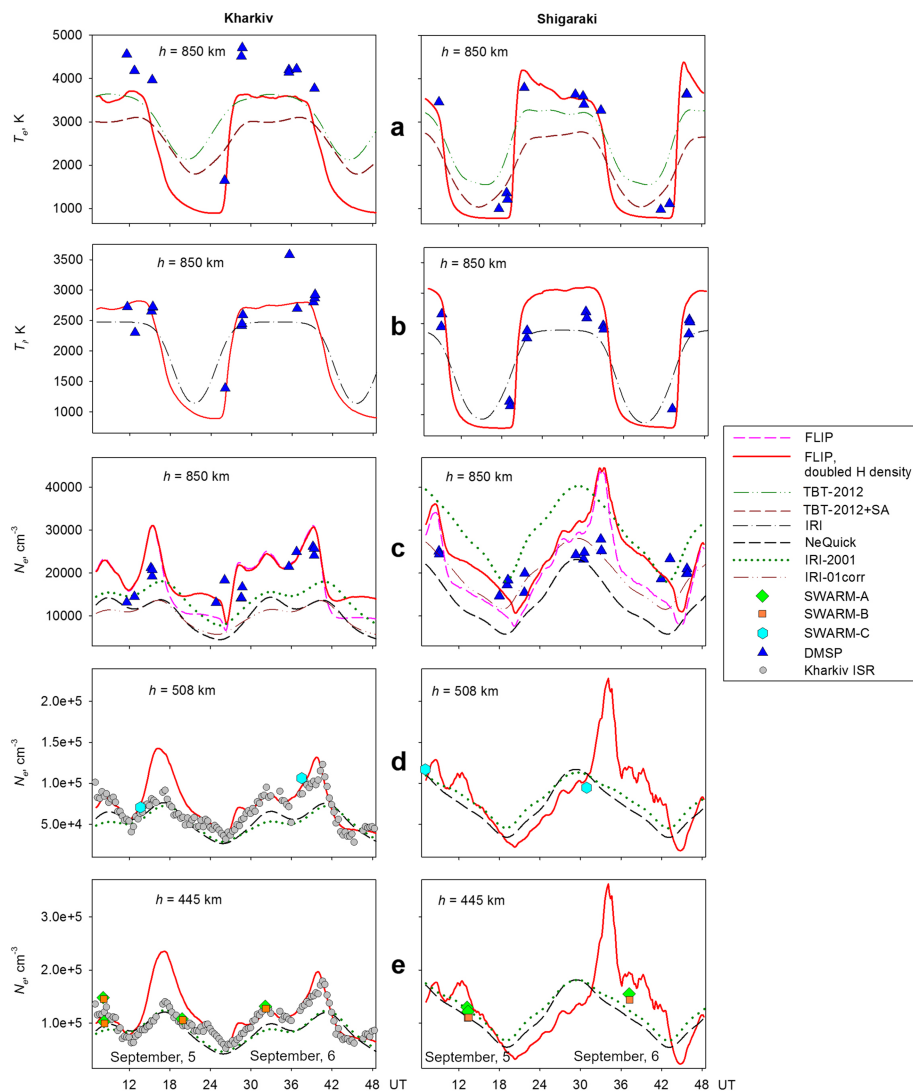


Fig. 4 Diurnal variations of electron and ion temperature, and electron density at 850 km (**a–c**), electron density at 508 km (**d**), and at 445 km (**e**). Solid red line is the FLIP model simulation with the $h_m F_2$ constraint together with doubled NRLMSISE-00 H density, dashed pink line – the same but with NRLMSISE-00 H density. Gray circles denote KhISR, blue triangles – DMSP, green diamonds – SWARM-A, orange squares – SWARM-B, cyan hexagons – SWARM-C observations respectively. On panel (**a**), dashed brown and dash-dotted green lines denote T_e variation from TBT-2012+SA and TBT-2012 models respectively. Dash-dotted black line on panel (**b**) shows T_i variation from IRI-2016 model. On panels (**c–e**), dashed black line denotes NeQuick, dotted green – IRI-2001, dash-dotted brown lines – IRI-01corr models calculations respectively. The models predictions and Kharkiv ISR data are 3-h averaged

For Shigaraki, several pre-sunrise DMSP data points in each of two nights agree better with the TBT-2012+SA model predictions (the model overestimates T_e by ~200–300 K); overestimation of T_e by TBT-2012 model reaches ~600 K.

The overall agreement of the IRI model with DMSP observations is much better for ion temperature (Fig. 4b). During the day, the IRI model overestimates T_i by several hundred kelvins. No reliable conclusion about the model-data agreement for the nighttime can be made due to the lack of data.

Electron density observations in the topside ionosphere were compared with three optional models of IRI at three altitudes (Fig. 4c–e). The default NeQuick model underestimates the DMSP N_e at 850 km in the European and Japanese sectors during the night by a factor of ~3. On the other hand, at the lower altitudes of 508 km and 445 km, the model-data agreement at night is excellent over Kharkiv. There were no data to compare with the NeQuick predictions over Shigaraki. During the daytime, the model-data agreement at 850 km is good for Shigaraki. For Kharkiv, the agreement is good for September 5 but

not for September 6 when NeQuick underestimates N_e by a factor of ~ 2 . Also, for this date, notable underestimation by NeQuick is seen for Kharkiv at 508 km (a factor of ~ 1.5) and at 445 km (a factor of ~ 1.3). For Shigaraki, daytime agreement of NeQuick with Swarm data point is excellent at 508 km.

The IRI-2001 model of N_e provides better predictions at 850 km for both longitudinal sectors and for both day and night compared with NeQuick. The model-data agreement is especially improved for Shigaraki while the underestimation is still a factor of ~ 1.5 for Kharkiv. At 508 km and 445 km altitudes, the IRI-2001 predictions are very close to those of the NeQuick model.

The IRI-01corr model predictions are the same as those of IRI-2001 at 445 km and 508 km. At 850 km, the IRI-01corr variation is close to that of the NeQuick model while for Shigaraki the IRI-01corr N_e variation lies approximately in the middle of the NeQuick and IRI-2001 variations.

3.3 Comparison of observations with FLIP physical model simulations

One of the key parameters for a successful simulation of the mid-latitude ionosphere is the diurnal variation of the horizontal thermospheric wind velocity, which is rarely available from data. The main effect of neutral winds is to change the entire electron density profile by changing the height (h_mF2) of the F2 density peak (N_mF2). Some global thermosphere physical models calculate wind vectors self-consistently and there are global empirical wind models. In both models, the velocity uncertainties are still too large for accurate ionosphere modeling (Drob et al. 2015). To overcome the wind uncertainty, the FLIP physical model uses an algorithm that adjusts the winds to accurately reproduce the observed h_mF2 as it steps in time (Richards 1991).

In this work, we present FLIP model simulations of F2-layer peak density with three types of input h_mF2 and with empirical models (Fig. 3). First, the h_mF2 input was the variation observed by the ISRs. At Kharkiv, this produced simulated N_mF2 variations that are in good agreement with the observations on September 6 (Fig. 3a). However, the model is up to a factor of ~ 2 too high at Kharkiv in the afternoon on September 5. For Shigaraki, the largest model-data disagreement is $\sim 40\%$ for the night of September 6.

The FLIP model with h_mF2 from the AMTB-2013 and SHU-2015 models produces overall good model-data agreement for Kharkiv and Shigaraki. The largest deviation is $\sim 100\%$ nighttime underestimation of N_mF2 over Kharkiv by FLIP with the SHU-2015 model. As in the case of using the ISR h_mF2 , the FLIP model overestimates N_mF2 for Kharkiv near sunset on September 5 by $\sim 80\%$ with both IRI models. Another difference is that the model

N_mF2 decay starts ~ 1.5 h too early in the evening of September 6 over Shigaraki. That is not the case when FLIP uses measured h_mF2 .

The final simulation was with the horizontal thermospheric winds from the HWM-14 model. For both longitudinal sectors the model-data agreement is worse than with any of the h_mF2 inputs. Over Kharkiv, using HWM-14 produces a $\sim 60\%$ overestimation of N_mF2 in the evening of September 6. Over Shigaraki, a factor of ~ 2 overestimation is seen for the nighttime.

For the model comparisons with the observations in the topside ionosphere that are shown in Fig. 4, the FLIP model was constrained to follow the ISR h_mF2 variations and the neutral hydrogen density in the NRLMSISE-00 atmospheric model was doubled in accordance with the recent findings of Kotov et al. (2015), (2016), (2018), and (2019) for the European region. It is seen that the calculated electron temperatures agree well with the DMSP observations excluding the morning hours of September 6 over Kharkiv when the model underestimated T_e by up to ~ 1000 K (Fig. 4a). There is also very good model-data agreement for the ion temperature (Fig. 4b) and electron density at all the three considered altitudes in both longitudinal sectors (Fig. 4c–d). As with N_mF2 , the exception is the evening of September 5 over Kharkiv where the model overestimates N_e by a factor of ~ 1.5 – 1.7 with the tendency of increasing model-data deviation with decreasing of altitude.

Additional simulations made with the NRLMSISE-00 standard neutral hydrogen density (Fig. 4c) clearly shows that the doubling of H density is really needed to provide matching the model to data not only for Kharkiv but for Shigaraki too.

3.4 Wave processes

Figure 5 demonstrates comparative results of wave characteristics and their localization in the temporal and periodical domains. Over both regions, we found an enhancement in the wave activity near the local solar terminator. Some increase in the power spectral density over Kharkiv also occurred near 09:00 and 16:00 LT, while that density was slightly amplified around 10:00 and 14:00 LT over Shigaraki (see Fig. 5b). Figure 5c shows the substantially downward phase progression. This is likely to indicate that majority of the TIDs are the ionospheric manifestations of internal gravity waves propagating from below.

Notably, the sunset terminator induced TIDs over Shigaraki at the same time that strong quasi-periodic fluctuations in h_mF2 ensued from the enhancement in magnetic activity (cf. Fig. 3, 34–38 UT that corresponds to 19–23 LT in Fig. 5). Separation of these two sources is facilitated by the difference in oscillation periods. As seen in Fig. 3, h_mF2 fluctuated with a predominant period of about 4 h, while that for the TIDs was about 80 min.

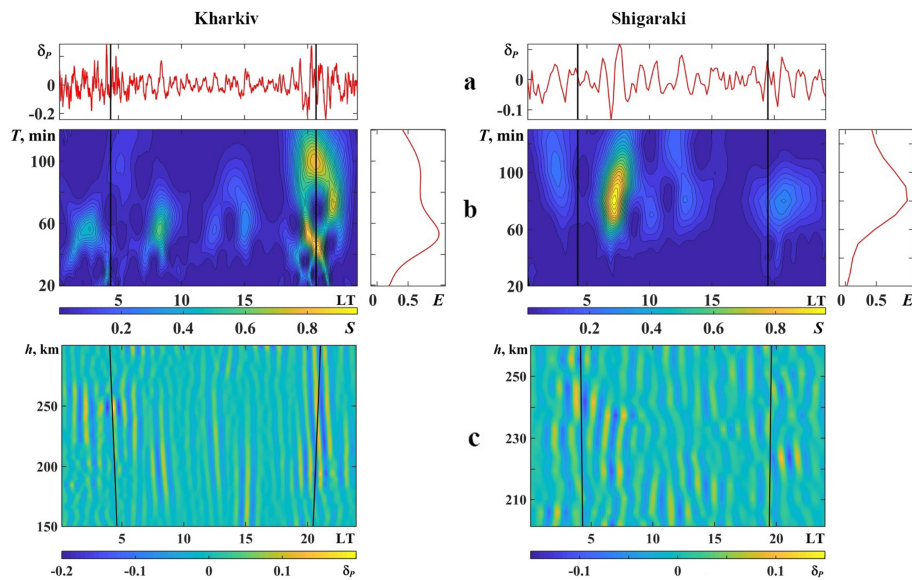


Fig. 5 Relative variations of incoherent scatter power δ_p (a) measured by KhISR at the altitude of 200 km (left) and MUR at the altitude of 220 km (right) as well as corresponding results of spectral analysis (b) and band-pass filtering (c). Subfigure (b) contains a power spectral density S indicated by color level plotted vs time and period as well as average power E plotted vs period. Both S and E values were normalized to their maximums. Subfigure (c) shows altitude-time plots of δ_p band-pass filtered in the range of 40–80 min and 60–120 min for KhISR and MUR data, respectively. The solid lines mark the time of local sunrise and sunset terminator passage at the current altitude. LT is solar apparent time

The main difference between these KhISR and MUR results is the greater value of predominant oscillation period over Japanese region. Indeed, as seen in the average power plots, the maximum values of $E(T)$ are attained at periods of about 50 min and 80 min over Kharkiv and Shigaraki, respectively. Unfortunately, the abrupt decrease in the SNR with altitude for the MUR data precludes an advanced comparative analysis of TID propagation such as an estimation of TID vertical and horizontal phase velocities as was done by Panasenko et al. (2019) in characterizing solar eclipse induced TIDs.

4 Discussion

This study provided an opportunity to assess the distinctive regional features of the ionospheric plasma variations in two distinct regions, to test capabilities of the empirical and physical models, and to compare the capabilities of different models and research facilities.

The observed differences between the daytime values of N_mF2 and T_e in the topside ionosphere over the European and Japanese longitudinal sectors are attributed to their magnetic latitudinal differences (45.5° for Kharkiv and 26.2° for Shigaraki). It is well known that the daytime N_mF2 is higher at low-to-middle latitudes than at mid-latitudes (e.g., Hoque and Jakowski (2011)), and this is the case for the Kharkiv and Shigaraki data. The higher daytime T_e values over Kharkiv agree with the commonly accepted knowledge that electron temperature increases with latitude (e.g., Truhlik et al. (2012)). The closeness of

the observed daytime T_i values in the topside ionosphere over the two regions is also consistent with our knowledge of global climatology for these parameters (Bilitza 1990). In contrast, the closeness of the topside N_e over Kharkiv and Shigaraki seen from DMSP data disagrees with the predictions of all three climatological N_e models which show a significant increase of the topside density towards lower latitudes (Bilitza 2004; Nava et al. 2008).

The rapid day to day changes in solar activity and series of moderate enhancements of magnetic activity on September 5–6 and on preceding days (see Fig. 1) make this period difficult for both physical and empirical models.

The h_mF2 predictions over Kharkiv and Shigaraki from the IRI models (AMTB-2013 and SHU-2015) follow the observations reasonably well but there are systematic deviations between the models and observations that can reach several tens of kilometers, which leads to unacceptable bias when N_mF2 is simulated by physical models. The HWM-14 model neutral winds significantly overestimate h_mF2 and N_mF2 most of the time in both regions. This may imply some bias in the thermospheric wind velocity of HWM-14 for the European and Japanese sectors during the period of the study.

However, even using of the measured h_mF2 variations as a neutral wind proxy for the FLIP model does not always guarantee better quality of N_mF2 reproduction. For example, the measured N_mF2 at Kharkiv is up to 50% lower for 12–18 UT than for 36–42 UT and such a low density

was not reproduced by the FLIP model. This is most likely because the NRLMSISE-00 model is underestimating the effect of the enhanced magnetic activity on the neutral composition during the preceding hours.

At Shigaraki, there is evidence of a weak magnetic disturbance that affects the F2-layer peak in the local evening (UT=32–34) of September 6 as indicated by the solid arrow in Fig. 3. The effect is clearly visible with h_mF2 rising reaching up to 60 km higher than on the previous evening (UT=8–10). The apparent cause of this behavior was the increase of AE from ~ 50 nT up to ~ 800 nT within ~ 3 h interval (at ~ 31 – 34 UT), which came following ~ 10 h of low magnetic activity. This significant uplifting over Shigaraki could be classified as a positive ionosphere storm from the passage of a traveling atmospheric disturbance (TAD) generated in the auroral zone. The FLIP model generates a clear rise in N_mF2 that would be expected from the TAD. The weaker increase in N_mF2 may be caused by storm related changes in neutral composition which were not correctly reflected by the NRLMSISE-00 model. It is interesting that the magnitude of the h_mF2 uplifting for Shigaraki is close to those obtained for the same (Asian) longitudinal sector in 1980s by Hajkowicz (1999). The FLIP model enhancement of electron density in the topside ionosphere over Shigaraki occurred just after the h_mF2 uplift. A similar enhancement was observed by KhISR and reproduced by the FLIP model for the similar event prior to sunset of September 25, 2016 (Kotov et al. 2019). The magnitudes of h_mF2 uplifting and related enhancements of N_mF2 and topside electron density were close to those we see here for Shigaraki.

The ionosphere over Kharkiv does not show similar TAD like behavior during this period (UT=32–34). This different ionosphere response could be a local time effect (e.g., Balan and Rao (1990)) either because of the longitude of the auroral impulse or the direction of the neutral wind. Towards the late afternoon, the thermospheric wind changes from poleward to equatorward. In such conditions, a magnetic disturbance may enhance the normal equatorward wind that leads to a more intense plasma uplifting along the magnetic field line. This behavior was less likely for Kharkiv where near-noon conditions normally correspond to a stable poleward wind. In such a case, a short-time enhancement of auroral activity was unable to produce a significant wind surge and uplift the ionosphere over Kharkiv.

In the topside ionosphere, the best agreement with the observations is with the FLIP physical model simulations for all the considered plasma parameters. Empirical models still need much improvement for describing the diurnal plasma parameter variation on a given day. This need is especially clear for the electron density models. None of the three N_e options of IRI can

provide acceptable agreement with the observations in either region. The models of electron temperature provide overly smoothed diurnal variations of T_e . Also, the model-data comparison reveals the need to increase the magnitude of day-to-night change of T_e in the IRI TBT-2012 model.

The direct electron density comparison of Swarm and Kharkiv ISR observations is the first such comparison for the European sector and for the typical magnetic mid-latitudes. All the previous comparisons (Lomidze et al. 2018) were made for American sector with the data of ISRs in Jicamarca (equatorial), Arecibo (low-middle), and Millstone Hill (sub-auroral). This comparison supports the high quality of Swarm electron density data for mid-latitudes.

An important new result from this study is that it provides evidence of the need to increase the neutral hydrogen density in NRLMSISE-00 model by at least a factor of 2 for the Japanese longitudinal sector (Fig. 4c). Such a need was previously deduced from different techniques for the American (Nossal et al. 2012, 2019) and European (Kotov et al. 2015, 2016, 2018, 2019) sectors. Here, we provide the first such evidence for Asian sector. This need should be validated by more model/data comparisons for different seasons and conditions.

The TID events observed over Kharkiv and Shigaraki were likely caused by the solar terminator passage because the enhancement in wave activity mostly occurred in the morning and evening hours (see Fig. 5). Thus, our results indicate that the solar terminator can be an effective source of ionospheric disturbances for different longitudinal regions. The detected TID periods are also in good agreement with the results of previous studies (see, e.g. Oliver et al. (1997); Song et al. (2013); Nygrén et al. (2015); Panasenko et al. (2018)). They exhibit a greater value for Japanese (about 80 min) than European (about 50 min) region. Notably, the very similar periodicities of 59 ± 11 min for large scaled TIDs over Europe (Borries et al. 2009) and 80 ± 29 min for those over Japan (Tsugawa et al. 2004) were reported. Such similarity could be simply a coincidence but could also reflect the regional features of wave processes and is the issue for further research.

5 Conclusions

This coordinated observational campaign using two incoherent scatter radars, two satellite missions, during 5–6 September of 2017 and appropriate model simulations provided the following key results.

1. The regular variations of the main plasma parameters at the F2-layer peak and in the topside ionosphere (electron density, electron and ion temperatures) for Kharkiv are close to those for Shigaraki qualitatively and quantitatively. Most of the slight differences seen from the

observations may be explained by the differences in their geomagnetic latitudes.

2. The International Reference Ionosphere empirical model is capable of predicting the qualitative features of the variations in the key ionospheric plasma parameters over Kharkiv and Shigaraki. However, the predictions still need to be improved quantitatively. None of the optional IRI sub-models of the F2-layer peak height, topside electron density, and temperature can be considered preferable.

3. The FLIP physical model provides the best agreement with the observations when being constrained to follow the observed diurnal variations of h_mF2 . Using the winds from the HWM-14 model in FLIP leads to an overestimation of h_mF2 during the whole day for both regions, which causes biases in N_mF2 calculations.

4. The high quality of Swarm electron density data is confirmed for the first time by a direct comparison with the ISR located at typical mid-latitudes (Kharkiv).

5. It was pointed that the rapid day to day changes in solar activity and series of moderate enhancements of magnetic activity on September 5–6 and in the preceding days made this period difficult for both physical and empirical modeling. The ionospheric response to the weak magnetic disturbance following ~10 h of magnetically quiet conditions (in the UT morning of September 6, 2017) was studied. Significant regional differences were found, apparently caused by the well-known LT effect of magnetic storms. This effect was confirmed by simulations with the FLIP model. The magnitude of the storm-induced h_mF2 enhancement observed over Shigaraki is found to be close to estimates obtained for the same longitudinal sector in 1980s by Hajkowicz (1999).

6. For the first time, evidence of a need to increase the neutral hydrogen density in NRLMSISE-00 model by a factor of at least 2 was obtained for the Asian longitudinal sector. More studies should be done to check if the same need is valid for other seasons and conditions.

7. Traveling ionospheric disturbances, likely induced by solar terminator passage, were detected over both Kharkiv and Shigaraki. They exhibit different dominant periods of about 50 min and 80 min over Europe and Japan, respectively. This could reflect differences in local time of occurrence as well as differences in latitude, longitude, and magnetic field inclination/declination that need to be further investigated.

Abbreviations

IT: Ionosphere and thermosphere; ISR: Incoherent scatter radar; IRI: International Reference Ionosphere; FLIP: Field Line Interhemispheric Plasma; KhISR: Kharkiv incoherent scatter radar; MUR: Middle and upper atmosphere radar; TID: Traveling ionospheric disturbance; DMSP: Defense Meteorological

Satellite Program; URSI: International Union of Radio Science; SNR: Signal-to-noise ratio; HWM: Horizontal wind model

Acknowledgements

We acknowledge Open Madrigal Initiative for providing DMSP data and personally thank Patricia Doherty (Boston College) and Marc Hairston (University of Texas at Dallas, W. B. Hanson Center for Space Sciences). The authors are grateful to the European Space Agency for Swarm data providing. The authors from Institute of ionosphere are thankful to Dr. L. Ya. Emelyanov and Ya. M. Chepurnyy for conducting KhISR observations.

Authors' contributions

SVP was a principal investigator of the collaborative project and analyzed the wave processes in both longitudinal sectors. DVK contributed to the concept of the study and participated in interpretation of the results on the neutral hydrogen density and storm-related effects. YO collaborated in this study and consulted about TID propagation. MY and HH organized MUR observations and consulted on MUR data analysis. PGR consulted on the simulations by FLIP model and participated in the interpretation of the FLIP based results. VT consulted on the empirical models and satellite data, participated in interpretation of the results. OVB developed the software for KhISR, MUR, Swarm, and DMSP data processing, as well as edited the manuscript in LaTeX. MOS conducted simulations by FLIP models and participated in the analysis of storm-related effects. TGZ manually analyzed all the ionograms and contributed in result discussion. IFD proposed a topic and designed a conception of the study. All authors read and approved the final manuscript.

Funding

SVP, DVK, YO, MY, HH, and PGR were supported by Collaborative Research based on the MU Radar and EAR Project "Coordinated observations of light ions and TIDs with Shigaraki MU and Kharkiv IS radars." The work of SVP and DVK was partially funded through a number of Ukrainian scientific projects (0117U004133, 0120U102038). OVB and MOS were supported by the project 0119U100032 "Investigations of long-term changes of the plasmasphere: new results for security into the space and on Earth" funded by the Ministry of Education and Science of Ukraine. VT was supported by grant LTAUSA17100 of the Ministry of Education, Youth and Sports of the Czech Republic.

Availability of data and materials

The ionospheric parameters based on rough analysis of KhISR data are available through the Institute of ionosphere Database (<http://database.iion.org.ua/>). The results of the thorough analysis of KhISR data can be obtained from SVP or DVK upon request. MUR data can be provided by MY and HH upon request. DMSP data are available at <http://cedar.openmadrigal.org>. Swarm data are obtained from <https://swarm-diss.eo.esa.int/>. The FLIP model laptop version is freely available from PGR upon request. International Reference Ionosphere model is available for on-line runs at https://ccmc.gsfc.nasa.gov/modelweb/models/iri2016_vitmo.php. Geomagnetic indices (A_p , K_p) are downloaded from the Space Weather Prediction Center data archive (ftp://ftp.swpc.noaa.gov/pub/indices/old_indices/). AE indices are taken at Goddard Space Flight Center SPDF site (<https://omniweb.gsfc.nasa.gov/>).

Declarations

Competing interests

The authors declare that they have no competing interests.

Author details

¹Institute of Ionosphere, 16 Kyrpychova, Kharkiv 61001, Ukraine. ²Institute for Space-Earth Environmental Research, Nagoya University, Furo-cho, Chikusa-ku, Nagoya City, Aichi Prefecture 464-8601, Japan. ³Research Institute for Sustainable Humanosphere, Kyoto University, Gokasho, Uji City, Kyoto Prefecture 611-0011, Japan. ⁴University of Alabama in Huntsville, Shelby Center for Science and Technology, 301 Sparkman Dr NW, Huntsville, AL 35899, USA. ⁵Institute of Atmospheric Physics of the Czech Academy of Science, Boční II 1401/1A, Prague 14100, Czech Republic.

Received: 19 March 2021 Accepted: 8 July 2021

Published online: 11 August 2021

References

- Altadill D, Magdaleno S, Torta J, Blanch E (2013) Global empirical models of the density peak height and of the equivalent scale height for quiet conditions. *Adv Space Res* 52(10):1756–1769. <https://doi.org/10.1016/j.asr.2012.11.018>
- Balan N, Otsuka Y, Bailey G, Fukao S (1998) Equinoctial asymmetries in the ionosphere and thermosphere observed by the MU radar. *J Geophys Res: Space Phys* 103(A5):9481–9495. <https://doi.org/10.1029/97JA03137>
- Balan N, Rao P (1990) Dependence of ionospheric response on the local time of sudden commencement and the intensity of geomagnetic storms. *J Atmos Terr Phys* 52(4):269–275. [https://doi.org/10.1016/0021-9169\(90\)90094-4](https://doi.org/10.1016/0021-9169(90)90094-4)
- Bent R, Llewellyn S, Schmid P (1972) Description and evaluation of the Bent ionospheric model, vol 1–3. National Information Service, Springfield, Virginia. Technical report, AD-753-081, -082, -083
- Bilitza D (1990) International Reference Ionosphere 1990, National Space Science Data Center. NSSDC/WDC-AR &S 90-22
- Bilitza D (2004) A correction for the IRI topside electron density model based on Alouette/ISIS topside sounder data. *Adv Space Res* 33(6):838–843. <https://doi.org/10.1016/j.asr.2003.07.009>
- Bilitza D, Altadill D, Zhang Y, Mertens C, Truhlik V, Richards P, McKinnell L-A, Reinisch B (2014) The International Reference Ionosphere 2012 – a model of international collaboration. *J Space Weather Space Clim* 4(A07). <https://doi.org/10.1051/swsc/2014004>
- Bilitza D, Eyfrig R, Sheikh N (1979) A global model for the height of the F2-peak using M3000 values from the CCIR numerical map. *ITU Telecommun J* 46:549–553
- Bogomaz O, Kotov D, Panasenکو S, Emelyanov L (2017) Advances in software for analysis of Kharkiv incoherent scatter radar data. In: 2017 International Conference on Information and Telecommunication Technologies and Radio Electronics (UkrMiCo). IEEE. pp 1–5. <https://doi.org/10.1109/UkrMiCo.2017.8095425>
- Booker HG (1977) Fitting of multi-region ionospheric profiles of electron density by a single analytic function of height. *J Atmos Terr Phys* 39(5):619–623. [https://doi.org/10.1016/0021-9169\(77\)90072-1](https://doi.org/10.1016/0021-9169(77)90072-1)
- Borries C, Jakowski N, Wilken V (2009) Storm induced large scale TIDs observed in GPS derived TEC. *Ann Geophys* 27(4):1605–1612. Copernicus GmbH
- Brace LH (1998) Langmuir probe measurements in the ionosphere. *Geophys Monogr-Am Geophys Union* 102:23–35. <https://doi.org/10.1029/GM102p0023>
- Buresova D, Lastovicka J, Hejda P, Bochnicek J (2014) Ionospheric disturbances under low solar activity conditions. *Adv Space Res* 54(2):185–196. <https://doi.org/10.1016/j.asr.2014.04.007>
- Chernogor LF (2008) Advanced methods of spectral analysis of quasiperiodic wave-like processes in the ionosphere: specific features and experimental results. *Geomagn Aeron* 48(5):652–673. <https://doi.org/10.1134/S0016793208050101>
- Chernogor LF (2011) The Earth–atmosphere–geospace system: main properties and processes. *Int J Remote Sens* 32(11):3199–3218. <https://doi.org/10.1080/01431161.2010.541510>
- Domnin IF, Chepurnyy YM, Emelyanov LY, Chernyaev SV, Kononenko AF, Kotov DV, Bogomaz OV, Iskra DA (2014) Kharkiv incoherent scatter facility. *Bulletin of the National Technical University “Kharkiv Polytechnic Institute”. Series “Radiophysics and ionosphere”* 471089:28–42
- Drob DP, Emmert JT, Meriwether JW, Makela JJ, Doornbos E, Conde M, Hernandez G, Noto J, Zawdie KA, McDonald SE, et al. (2015) An update to the Horizontal Wind Model (HWM): the quiet time thermosphere. *Earth Space Sci* 2(7):301–319. <https://doi.org/10.1002/2014EA000089>
- England S, Maus S, Immel T, Mende S (2006) Longitudinal variation of the E-region electric fields caused by atmospheric tides. *Geophys Res Lett* 33(21). <https://doi.org/10.1029/2006GL027465>
- Evans J (1969) Theory and practice of ionosphere study by Thomson scatter radar. *Proc IEEE* 57(4):496–530. <https://doi.org/10.1109/PROC.1969.7005>
- Fukao S, Sato T, Tsuda T, Kato S, Wakasugi K, Makihiro T (1985) The MU radar with an active phased array system: 1. Antenna and power amplifiers. *Radio Sci* 20(6):1155–1168. <https://doi.org/10.1029/RS020i006p01155>
- Fukao S, Tsuda T, Sato T, Kato S, Wakasugi K, Makihiro T (1985) The MU radar with an active phased array system: 2. In-house equipment. *Radio Sci* 20(6):1169–1176. <https://doi.org/10.1029/RS020i006p01169>
- Fuller-Rowell T, Araujo-Pradere E, Codrescu M (2000) An empirical ionospheric storm-time correction model. *Adv Space Res* 25(1):139–146. [https://doi.org/10.1016/S0273-1177\(99\)00911-4](https://doi.org/10.1016/S0273-1177(99)00911-4)
- Fuller-Rowell T, Codrescu M, Araujo-Pradere E, Kutiev I (1998) Progress in developing a storm-time ionospheric correction model. *Adv Space Res* 22(6):821–827. [https://doi.org/10.1016/S0273-1177\(98\)00105-7](https://doi.org/10.1016/S0273-1177(98)00105-7)
- Hairston MR, Mrak S, Coley W, Burrell A, Holt B, Perdue M, Depew M, Power R (2018) Topside ionospheric electron temperature observations of the 21 August 2017 eclipse by DMSP spacecraft. *Geophys Res Lett* 45(15):7242–7247. <https://doi.org/10.1029/2018GL077381>
- Hajkowicz LA (1999) Monitoring ionospheric response to auroral electrojet activity from sub-auroral to equatorial latitudes in the East Asian-Australian longitudinal sector over a solar cycle (1978–1986). *J Atmos Sol-Terr Phys* 61(11):857–866. [https://doi.org/10.1016/S1364-6826\(99\)00034-6](https://doi.org/10.1016/S1364-6826(99)00034-6)
- Hapgood M (2011) Towards a scientific understanding of the risk from extreme space weather. *Adv Space Res* 47(12):2059–2072. <https://doi.org/10.1016/j.asr.2010.02.007>
- Hassenpflug G, Yamamoto M, Luce H, Fukao S (2008) Description and demonstration of the new middle and upper atmosphere radar imaging system: 1-D, 2-D, and 3-D imaging of troposphere and stratosphere. *Radio Sci* 43(02):1–24. <https://doi.org/10.1029/2006RS003603>
- Heelis R (2004) Electrodynamics in the low and middle latitude ionosphere: a tutorial. *J Atmos Sol-Terr Phys* 66(10):825–838
- Heelis R, Hanson W (1998) Measurements of thermal ion drift velocity and temperature using planar sensors. *Geophys Monogr-Am Geophys Union* 102:61–72
- Hoque MM, Jakowski N (2011) A new global empirical NmF2 model for operational use in radio systems. *Radio Sci* 46(06):RS6015. <https://doi.org/10.1029/2011RS004807>
- Kim E, Jee G, Ji E-Y, Kim YH, Lee C, Kwak Y-S, Shim J-S (2020) Climatology of polar ionospheric density profile in comparison with mid-latitude ionosphere from long-term observations of incoherent scatter radars: A review. *J Atmos Sol-Terr Phys*:105449
- Knudsen D, Burchill J, Buchert S, Eriksson A, Gill R, Wahlund J-E, Åhlén L, Smith M, Moffat B (2017) Thermal ion imagers and Langmuir probes in the Swarm electric field instruments. *J Geophys Res: Space Phys* 122(2):2655–2673. <https://doi.org/10.1002/2016JA022571>
- Kotov D, Richards P, Bogomaz O, Chernogor L, Truhlik V, Emelyanov LY, Chepurnyy YM, Domnin I (2016) The importance of neutral hydrogen for the maintenance of the midlatitude winter nighttime ionosphere: evidence from IS observations at Kharkiv, Ukraine, and field line interhemispheric plasma model simulations. *J Geophys Res: Space Phys* 121(7):7013–7025. <https://doi.org/10.1002/2016JA022442>
- Kotov D, Richards PG, Truhlik V, Bogomaz O, Shulha M, Maruyama N, Hairston M, Miyoshi Y, Kasahara Y, Kumamoto A, et al. (2018) Coincident observations by the Kharkiv IS radar and ionosonde, DMSP and Arase (ERG) satellites, and FLIP model simulations: implications for the NRLMSISE-00 hydrogen density, plasmasphere, and ionosphere. *Geophys Res Lett* 45(16):8062–8071. <https://doi.org/10.1029/2018GL079206>
- Kotov D, Richards PG, Truhlik V, Maruyama N, Fedrizzi M, Shulha M, Bogomaz O, Lichtenberger J, Hernández-Pajares M, Chernogor L, et al. (2019) Weak magnetic storms can modulate ionosphere-plasmasphere interaction significantly: mechanisms and manifestations at mid-latitudes. *J Geophys Res: Space Phys* 124(11):9665–9675. <https://doi.org/10.1029/2019JA027076>
- Kotov DV, Truhlik V, Richards PG, Stankov S, Bogomaz OV, Chernogor LF, Domnin IF (2015) Night-time light ion transition height behaviour over the Kharkiv (50 N, 36 E) IS radar during the equinoxes of 2006–2010. *J Atmos Sol-Terr Phys* 132:1–12. <https://doi.org/10.1016/j.jastp.2015.06.004>
- Liu Z, Fang H, Weng L, Wang S, Niu J, Meng X (2019) A comparison of ionosonde measured foF2 and IRI-2016 predictions over China. *Adv Space Res* 63(6):1926–1936. <https://doi.org/10.1016/j.asr.2019.01.017>
- Lomidze L, Knudsen DJ, Burchill J, Kouznetsov A, Buchert SC (2018) Calibration and validation of swarm plasma densities and electron temperatures using ground-based radars and satellite radio occultation measurements. *Radio Sci* 53(1):15–36. <https://doi.org/10.1002/2017RS006415>
- Luan X, Dou X (2013) Seasonal dependence of the longitudinal variations of nighttime ionospheric electron density and equivalent winds at southern midlatitudes. *Ann Geophys* 31:1699–1708. <https://doi.org/10.5194/angeo-31-1699-2013>
- Nava B, Coisson P, Radicella S (2008) A new version of the nequick ionosphere electron density model. *J Atmos Sol-Terr Phys* 70(15):1856–1862. <https://doi.org/10.1016/j.jastp.2008.01.015>

- Nossal S, Mierkiewicz E, Roesler F (2012) Observed and modeled solar cycle variation in geocoronal hydrogen using NRLMSISE-00 thermosphere conditions and the bishop analytic exosphere model. *J Geophys Res: Space Phys* 117(A3). <https://doi.org/10.1029/2011JA017074>
- Nossal S, Mierkiewicz E, Roesler F, Woodward R, Gardner D, Haffner L (2019) Geocoronal hydrogen emission variation over two solar cycles. *J Geophys Res: Space Phys* 124(12):10674–10689. <https://doi.org/10.1029/2019JA026903>
- Nygrén T, Aikio AT, Voiculescu M, Cai L (2015) Radar observations of simultaneous traveling ionospheric disturbances and atmospheric gravity waves. *J Geophys Res: Space Phys* 120(5):3949–3960. <https://doi.org/10.1002/2014JA020794>
- Oliver WL, Otsuka Y, Sato M, Takami T, Fukao S (1997) A climatology of F region gravity wave propagation over the middle and upper atmosphere radar. *J Geophys Res* 102:14499–14512. <https://doi.org/10.1029/97JA00491>
- Panasenko SV, Goncharenko LP, Erickson PJ, Aksonova KD, Domin IF (2018) Traveling ionospheric disturbances observed by Kharkiv and Millstone Hill incoherent scatter radars near vernal equinox and summer solstice. *J Atmos Sol-Terr Phys* 172:10–23. <https://doi.org/10.1016/j.jastp.2018.03.001>
- Panasenko SV, Otsuka Y, van de Kamp M, Chernogor LF, Shinbori A, Tsugawa T, Nishioka M (2019) Observation and characterization of traveling ionospheric disturbances induced by solar eclipse of 20 March 2015 using incoherent scatter radars and GPS networks. *J Atmos Sol-Terr Phys* 191:105051. <https://doi.org/10.1016/j.jastp.2019.05.015>
- Patel N, Karia S, Pathak K (2019) Evaluation of the improvement of IRI-2016 over IRI-2012 at the India low-latitude region during the ascending phase of cycle 24. *Adv Space Res* 63(6):1860–1881. <https://doi.org/10.1016/j.asr.2018.10.008>
- Pirog O, Polekh N, Chistyakova L (2001) Longitudinal variation of critical frequencies in polar F-region. *Adv Space Res* 27(8):1395–1398. [https://doi.org/10.1016/S0273-1177\(01\)00038-2](https://doi.org/10.1016/S0273-1177(01)00038-2)
- Rich F (1994) Users guide for the topside ionospheric plasma monitor (SSIES, SSIES-2 and SSIES-3) on spacecraft of the Defense Meteorological Satellite Program, Volume 1: Technical description. Technical report, Air Force Phillips Laboratory, Hanscom AFB. <https://apps.dtic.mil/sti/pdfs/ADA315731.pdf>
- Richards P (1991) An improved algorithm for determining neutral winds from the height of the F2 peak electron density. *J Geophys Res: Space Phys* 96(A10):17839–17846. <https://doi.org/10.1029/91JA01467>
- Richards P (2001) Seasonal and solar cycle variations of the ionospheric peak electron density: comparison of measurement and models. *J Geophys Res: Space Phys* 106(A7):12803–12819. <https://doi.org/10.1029/2000JA000365>
- Richards P, Meier R, Chen S-P, Drob D, Dandenault P (2017) Investigation of the causes of the longitudinal variation of the electron density in the Weddell Sea Anomaly. *J Geophys Res: Space Phys* 122(6):6562–6583. <https://doi.org/10.1002/2016JA023565>
- Richards P, Meier R, Wilkinson P (2010) On the consistency of satellite measurements of thermospheric composition and solar EUV irradiance with Australian ionosonde electron density data. *J Geophys Res: Space Phys* 115(A10). <https://doi.org/10.1029/2010JA015368>
- Rush C (1989) Ionospheric mapping—an update of foF2 coefficients. *Telecomm J* 56:179–182
- Sagawa E, Immel T, Frey H, Mende S (2005) Longitudinal structure of the equatorial anomaly in the nighttime ionosphere observed by IMAGE/FUV. *J Geophys Res: Space Phys* 110(A11). <https://doi.org/10.1029/2004JA010848>
- Schunk RW, Scherliess L, Eccles V, Gardner L, Sojka JJ, Zhu L, Pi X, Mannucci A, Wilson B, Kornjathy A, et al. (2014) Ensemble modeling with data assimilation models: a new strategy for space weather specifications, forecasts, and science. *Space Weather* 12(3):123–126. <https://doi.org/10.1002/2014SW001050>
- Shubin V (2015) Global median model of the F2-layer peak height based on ionospheric radio-occultation and ground-based Digisonde observations. *Adv Space Res* 56(5):916–928. <https://doi.org/10.1016/j.asr.2015.05.029>
- Song Q, Ding F, Wan W, Ning B, Liu L, Zhao B, Li Q, Zhang R (2013) Statistical study of large-scale traveling ionospheric disturbances generated by the solar terminator over China. *J Geophys Res: Space Phys* 118(7):4583–4593. <https://doi.org/10.1002/jgra.50423>
- Truhlik V, Bilitza D, Triskova L (2012) A new global empirical model of the electron temperature with the inclusion of the solar activity variations for IRI. *Earth Planets Space* 64(6):531. <https://doi.org/10.5047/eps.2011.10.016>
- Truhlik V, Trisková L, Šmilauer J (2001) Improved electron temperature model and comparison with satellite data. *Adv Space Res* 27(1):101–109. [https://doi.org/10.1016/S0273-1177\(00\)00144-7](https://doi.org/10.1016/S0273-1177(00)00144-7)
- Tsugawa T, Saito A, Otsuka Y (2004) A statistical study of large-scale traveling ionospheric disturbances using the GPS network in Japan. *J Geophys Res: Space Phys* 109(A6). <https://doi.org/10.1029/2003JA010302>
- Tsurutani BT, Verkhoglyadova OP, Mannucci AJ, Lakhina GS, Huba JD (2012) Extreme changes in the dayside ionosphere during a Carrington-type magnetic storm. *J Space Weather Space Clim* 2:05. <https://doi.org/10.1051/swsc/2012004>
- Zhang S, Coster AJ, Holt JM, Foster JC, Erickson P (2012) Ionospheric longitudinal variations at midlatitudes: incoherent scatter radar observation at Millstone Hill. *Sci China Technol Sci* 55(5):1153–1160. <https://doi.org/10.1007/s11431-012-4784-y>
- Zhang S-R, Foster JC, Coster AJ, Erickson PJ (2011) East-West Coast differences in total electron content over the continental US. *Geophys Res Lett* 38(19):L19101. <https://doi.org/10.1029/2011GL049116>

Publisher's Note

Springer Nature remains neutral with regard to jurisdictional claims in published maps and institutional affiliations.

Submit your manuscript to a SpringerOpen[®] journal and benefit from:

- Convenient online submission
- Rigorous peer review
- Open access: articles freely available online
- High visibility within the field
- Retaining the copyright to your article

Submit your next manuscript at ► [springeropen.com](https://www.springeropen.com)